Hypercontractile mutant of ventricular myosin essential light chain leads to disruption of sarcomeric structure and function and results in restrictive cardiomyopathy in mice

Chen-Ching Yuan[1], Katarzyna Kazmierczak[1], Jingsheng Liang[1], Rosemeire Kanashiro-Takeuchi[1], Thomas C. Irving[2], Aldrin V. Gomes[3], Yihua Wang[4], Thomas P. Burghardt[4], and Danuta Szczesna-Cordary[1]*

[1]Molecular and Cellular Pharmacology, University of Miami Miller School of Medicine, Miami, FL 33136, USA; [2]Illinois Institute of Technology, Chicago, IL 60616, USA; [3]Department of Neurobiology, Physiology and Behavior, University of California, Davis, CA 95616, USA; and [4]Department of Biochemistry and Molecular Biology, Mayo Clinic Rochester, Rochester, MN 55905, USA

Aims	The E143K (Glu → Lys) mutation in the myosin essential light chain has been associated with restrictive cardiomyopathy (RCM) in humans, but the mechanisms that underlie the development of defective cardiac function are unknown. Using transgenic E143K-RCM mice, we sought to determine the molecular and cellular triggers of E143K-induced heart remodelling.
Methods and results	The E143K-induced abnormalities in cardiac function and morphology observed by echocardiography and invasive haemodynamics were paralleled by augmented active and passive tension measured in skinned papillary muscle fibres compared with wild-type (WT)-generated force. *In vitro*, E143K-myosin had increased duty ratio and binding affinity to actin compared with WT-myosin, increased actin-activated ATPase activity and slower rates of ATP-dependent dissociation of the acto-myosin complex, indicating an E143K-induced myosin hypercontractility. E143K was also observed to reduce the level of myosin regulatory light chain phosphorylation while that of troponin-I remained unchanged. Small-angle X-ray diffraction data showed a decrease in the filament lattice spacing ($d_{1,0}$) with no changes in the equatorial reflections intensity ratios ($I_{1,1}/I_{1,0}$) in E143K vs. WT skinned papillary muscles. The hearts of mutant-mice demonstrated ultrastructural defects and fibrosis that progressively worsened in senescent animals and these changes were hypothesized to contribute to diastolic disturbance and to mild systolic dysfunction. Gene expression profiles of E143K-hearts supported the histopathology results and showed an upregulation of stress-response and collagen genes. Finally, proteomic analysis evidenced RCM-dependent metabolic adaptations and higher energy demands in E143K vs. WT hearts.
Conclusions	As a result of the E143K-induced myosin hypercontractility, the hearts of RCM mice model exhibited cardiac dysfunction, stiff ventricles and physiological, morphologic, and metabolic remodelling consistent with the development of RCM. Future efforts should be directed toward normalization of myosin motor function and the use of myosin-specific therapeutics to avert the hypercontractile state of E143K-myosin and prevent pathological cardiac remodelling.
Keywords	Cardiac myosin essential light chain • Diastolic and systolic dysfunction • Hypercontractility • Myosin step size • Proteomics

---

* Corresponding author. Tel: +1 305 2432908; fax: +1 305 2434555, E-mail: dszczesna@med.miami.edu

1. Introduction

There are three major types of cardiomyopathy: hypertrophic (HCM), dilated (DCM), and restrictive (RCM), with RCM being the least common and ultimately the least studied.[1] RCM is a heterogeneous disorder that can present with a spectrum of cardiac phenotypes including HCM in family members.[2–4] The prognosis for RCM has been poor and some patients die in childhood.[5] RCM is characterized by increased stiffness of the left ventricular (LV) wall with no increase in wall thickness and a largely impaired diastolic function with usually normal or near-normal systolic function.[3] RCM is rare in children, but the prognosis is poor and the risk for ischemia-related complications and death is high.[6]

RCM has been associated with several mutations in sarcomeric proteins, including troponin-I (TnI), troponin-T (TnT), actin, myosin binding protein C and β-myosin heavy chain (β-MHC).[7,8] In this study, we report on the first myosin essential light chain (ELC) mutation, E143K, where glutamic acid (E) is mutated to lysine (K), reported to result in HCM of restrictive physiology in humans.[9,10] In the first report, the mutation was discovered in a young male proband, homozygous for E143K during his medical evaluation due to the pre-mature death of his two younger siblings.[10] Another incidence of early death, at 7 years of age, was also reported in distant branch of the family. All family members homozygous for E143K manifested severe HCM in childhood.[10] In the second study, E143K was found in a 22 year-old female proband diagnosed with RCM and class III/IV heart failure while awaiting heart transplantation.[9] Transthoracic echocardiogram evaluation of the proband revealed a severe biatrial enlargement with preserved biventricular systolic function and no LV hypertrophy, while the Doppler interrogation indicated advanced LV diastolic dysfunction.[9] The lack of LV hypertrophy was paralleled by elevated right-sided and left-sided filling pressures and interstitial fibrosis.

To address the mechanism underlying the development of ELC-RCM phenotype, we generated transgenic (Tg) mice expressing the E143K-mutated human ventricular myosin ELC, the first animal model of human RCM with a mutation in myosin light chains, and the first RCM Tg murine model with a mutation in the thick filaments. Despite ∼55% of E143K expression, we were able to recapitulate the major aspects of the human phenotype, whereas E143K-positive patients displayed the RCM symptoms only when both alleles were mutated.[10] Male (M) and female (F) E143K mice manifested diastolic disturbance, especially in senescent animals, with ultrastructural cardiac defects and fibrosis that most likely contributed to mild systolic dysfunction. At the level of myosin molecules, a hypercontractile E143K-phenotype was observed evidenced by enhanced binding of myosin to actin in rigor, elevated actin-activated myosin ATPase activity and E143K-induced increase in the myosin duty ratio. Importantly, myosin RLC phosphorylation, shown to be critical for the normal function of the heart, was reduced in E143K-ELC mice. Finally, proteomic investigations revealed significant alterations in the metabolic processes involving ATP production and changes in the expression of energy related mitochondrial proteins.

2. Methods

This study conforms to the Guide for the Care and Use of Laboratory Animals published by the US National Institutes of Health (NIH Publication no. 85-23, revised 2011). All protocols were approved by the Institutional Animal Care and Use Committee at the University of Miami Miller School of Medicine. The assurance number is #A-3224-01,

effective November 24, 2015. Euthanasia of mice was achieved through inhalation of CO_2 followed by cervical dislocation.

The generation and characterization of Tg-mice expressing the human cardiac myosin ELC WT (NCBI accession number: P08590) used in this study was described earlier.[11–13] The same methodology was used to generate Tg-E143K mice (L1 and L2 expressing 0 and ∼55% transgene, respectively, and the results were compared with those obtained for Tg-WT L4 expressing 74% of human ventricular WT-ELC, as determined in cardiac myofibrils from three age groups (2–3, 5–6, and 10–11 mo-old) of mutant vs. WT-ELC mice (see Supplementary material online, *Figure S1*).

The paraffin-embedded longitudinal sections of whole mouse hearts, stained with haematoxylin and eosin and Masson's trichrome, were examined for overall morphology and fibrosis, and the myocardial ultrastructure was assessed by transmission electron microscopy as described earlier.[14] Hydroxyproline (HOP) content was determined using the HOP assay and the collagen and stress response gene profiles were assessed by real time qPCR.[12]

Cardiac morphology and function were examined in 5–6 and 11–12 mo-old male (M) and female (F) E143K and WT mice by echocardiography, invasive haemodynamics and muscle fibre mechanics studies.[11,14] Steady-state force development, force-pCa relationship, passive tension and small-angle X-ray diffraction experiments on skinned papillary muscles were conducted as described earlier.[13,14] Binding of E143K-mouse myosin to pyrene-actin, actin-activated myosin ATPase activity and stopped-flow kinetics were performed as previously reported.[11,13] *In vitro* motility and Qdot assays, followed by simulations of data ensembles, were conducted as outlined earlier.[15–17] Proteomics experiments on the hearts from E143K vs. WT mice were carried out according to Gomes *et al.*[18]

All values are shown as means ± SEM (standard error of the mean). Statistically significant differences between two groups were determined using an unpaired Student's *t*-test, with significance defined as *$P < 0.05$ and **$P < 0.01$. Comparisons between multiple groups were performed using one- or two-way ANOVA. Statistical procedures of the motility and Qdot assays and proteomic experiments are described in the Supplementary material online.

Details of materials and experimental procedures are in the Methods in the Online Data Supplement.

3. Results

This report focuses on the mechanisms by which the first RCM-linked mutation in myosin ELC regulates the development of RCM in mice. Using the cardiac specific α-MHC promoter,[11,12] E143K-L1 and E143K-L2 mice were produced expressing 0 and ∼55%, respectively, of the human ventricular ELC-E143K mutant protein in the hearts of mice. Western blots analysis performed on cardiac myofibrils from left ventricles of 2–3, 5–6, and 10–11 mo-old E143K-L2-mice and probed with monoclonal ELC-specific antibody (ab680, Abcam) is presented in Supplementary material online, *Figure S1*. A slightly lower expression was observed in the youngest E143K mice (∼51%) but no differences were noted between 5–6 (∼58%) and 10–11 (∼56%) mo-old E143K-mice. No differences in any age group were observed between male and female mice. The results obtained for E143K-L2 animals were compared with age and gender matched WT mice,[11] expressing ∼74% of the human ventricular ELC (see Supplementary material online, *Figure S1*).

3.1 LV fibrosis and ultrastructural defects in E143K-hearts

Histopathological evaluation of 5–6 mo-old and 11–12 mo-old E143K animals showed mild fibrosis in the hearts of younger group of mice of both genders, but severe fibrotic lesions in older mutant hearts compared with respective WT controls (*Figure 1A*). Myocardial ultrastructure assessed by transmission EM revealed significant sarcomere irregularities with Z-lines streaming and M-lines vanishing in ∼11 mo-old E143K-mice compared with WT hearts (*Figure 1B*). In support of histopathology findings, a significant increase in HOP content was measured in the hearts of ∼11 mo-old E143K vs. WT mice by HOP assay: 18.46 ± 1.22 vs. $15.09 \pm 0.43 \mu M/mg$ (*t-test*, *$P < 0.05$) (*Figure 1C*). Occurrences of fibrosis in E143K-hearts were confirmed by real-time PCR, showing upregulation of collagen type-I and III and a stress response gene, ANF, in ∼6 mo-old E143K mice compared with age-matched WT-controls. Additionally, α-MHC (*Myh6* gene) was significantly downregulated in E143K hearts compared with WT hearts (*Figure 1C*). Downregulation of α-MHC observed in E143K mice did not coincide with increased β-MHC protein expression in E143K vs. WT mice (see Supplementary material online, *Figure S2*); however, the possibility exists that the relative content of β-MHC in total MHC was increased in E143K hearts.

3.2 Diastolic dysfunction without LV hypertrophy in E143K mice

The *in vivo* consequences associated with E143K-ELC were assessed by echocardiography and invasive haemodynamics performed on 5–6 and 11–12 mo-old E143K vs. WT mice of both genders. Consistent with the RCM phenotype with preserved systolic function,[3,5] no differences were noted in the ejection fraction (EF in %) and fractional shortening (FS in %) in the young and old E143K vs. WT mice (*Figures 2–3*, see Supplementary material online, *Tables S1* and *S2*). The hearts of E143K animals did not show any hypertrophic growth compared with age matched controls, and on the contrary, the heart weight-to-body weight ratio was significantly lower in 5–6 mo-old E143K mice of both genders (*Figure 2A*, see Supplementary material online, *Table S1*) and in 11–12 mo-old E143K-M mice (*Figure 3A*, see Supplementary material online, *Table S2*) compared with respective WT controls. Additionally, LV inner diameters (LVID) in diastole and systole were smaller in young and old E143K-M than in WT-M mice indicating a more pronounced RCM phenotype in male vs. female mutant mice.

Haemodynamic evaluation showed a significant decrease in stroke volume (SV) with a decline in LV end-diastolic volume (EDV) and reduced cardiac output (CO) in 5–6 mo-old E143K-M mice, while female counterparts showed a significant increase in the relaxation time, Tau compared with respective WT controls (*Figure 2B*). The values of the peak rate of LV relaxation (-dP/dt$_{min}$) were lower in M and F E143K animals compared with age and gender matched WT mice and although the differences did not reach statistical significance, the trend of changes in E143K animals was suggestive of diastolic disturbance (*Figure 2B*, see Supplementary material online, *Table S1*). These data indicated that 5–6 mo-old E143K mice of both genders were pre-disposed to diastolic dysfunction.

Evaluation of 11–12 mo-old mutant vs. WT mice revealed a more pronounced phenotype in male vs. female E143K compared with WT mice (*Figure 3*, see Supplementary material online, *Table S2*), a trend also observed in other animal models of heart disease.[19] The mitral valve Doppler assessment showed a significant increase in the isovolumetric relaxation time (IVRT) in E143K-M mice compared with WT-M animals.

However, the diastolic indices, end-diastolic pressure (EDP), Tau and EDPVR were significantly altered (higher) in 11–12 mo-old E143K mice of both genders compared with age and gender matched WT animals, showing a pre-disposition of old E143K-mice to diastolic dysfunction (*Figure 3B*, see Supplementary material online, *Table S2*). The systolic indices, CO, SV, ESV, and EDV were significantly reduced in older E143K-M compared with WT-M mice, but female mice showed a significant reduction in stroke work (SW) compared with age matched WT-F animals. In addition, ESPVR (slope of the end-systolic PV relation) in E143K-M mice and PRSW (pre-load recruited SW-slope of the SW-EDV relationship) in E143K-F mice were significantly lower compared with respective WT controls, indicating impairment of systolic function in old mutant animals (*Figure 3B*, see Supplementary material online, *Table S2*). Although the pre-dominant phenotype observed in M and F senescent E143K animals was diastolic dysfunction, the mutation also resulted in a mild systolic disturbance compared with age and gender matched WT controls.

3.3 Hypercontractility and increased ventricular stiffness in E143K-skinned fibers

Papillary muscle strips were isolated from 5 to 6 mo-old and 11 to 12 mo-old mice, dissected to ∼1.5 mm in length and ∼100 μm in diameter, attached to a Guth force transducer and the sarcomere length was adjusted to 2.1 μm.[20] After maximal force determination in pCa 4 solution, the strips were exposed to solutions of increasing concentration of Ca^{2+} (pCa 8–4) and the force-[Ca^{2+}] relationship was established (see Supplementary material online, for details). As shown in *Figure 4A*, significantly increased maximal force was observed for fibres from 5 to 6 mo-old E143K-M and 11 to 12 mo-old E143K-F/M mice compared with respective WT mice, but only E143K-M mice demonstrated a small increase in the Ca^{2+}-sensitivity of force. Therefore, consistent with the *in vivo* evaluation, a more pronounced RCM phenotype was observed in skinned muscle fibres from male vs. female mutant mice (*Figure 4B*). It is important to note that fibrosis and ultrastructural defects observed in LV walls of ∼11 mo-old E143K hearts (*Figure 1A, B*) were most likely absent in the papillary muscles of E143K mice that were used for functional mechanical measurements. As we demonstrated previously,[21] LV papillary muscles of 2, 3, and 12.5 mo-old HCM mice maintained normal morphology, with no obvious myofibrillar disarray and interstitial fibrosis that we found abundant in LV and IVS compartments of mutant animals[21] and observed in E143K mice (*Figure 1A, B*). Thus, increased tension measured in E143K papillary muscles was most likely due to the hypercontractile activity of myosin motor and was not affected by sarcomere damage in old E143K mice.

The ability of myosin to generate force in E143K mice correlated with the results from small angle X-ray diffraction studies showing significantly reduced interfilament lattice spacing ($d_{1,0}$) measured under relaxation conditions in E143K-fibers compared with WT (*Figure 4C*). Consistent with this result, the level of passive tension (at pCa 8) in response to muscle stretch was significantly increased in E143K vs. WT mice (*Figure 4D*). Therefore, in agreement with functional assessments of E143K-hearts, abnormal muscle stiffness was observed in our RCM-ELC mouse model.

3.4 Enhanced interaction of mutant-myosin with actin

Binding of E143K vs. WT myosin to pyrene-F-actin under rigor conditions (no ATP) showed two different profiles for the mutant and WT
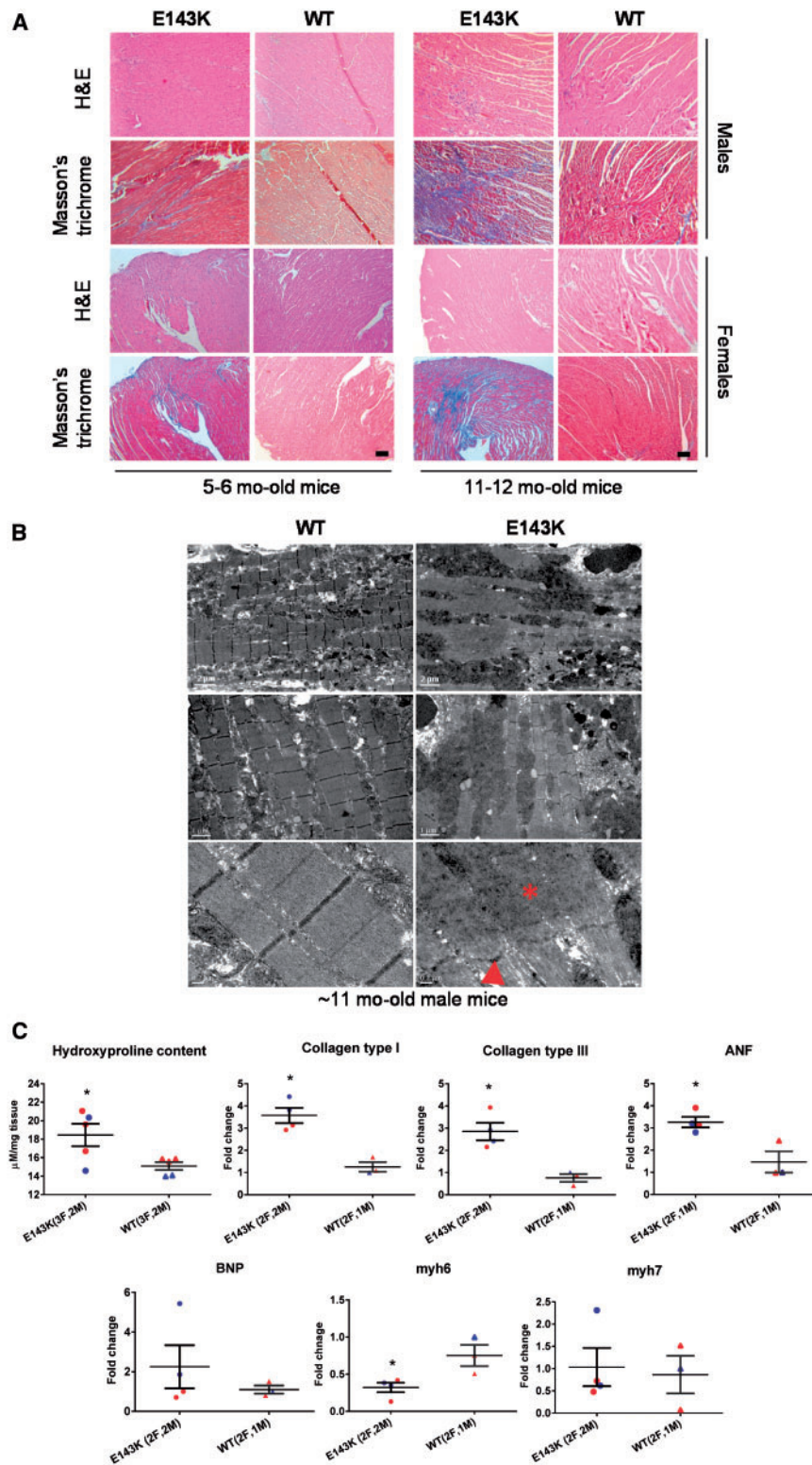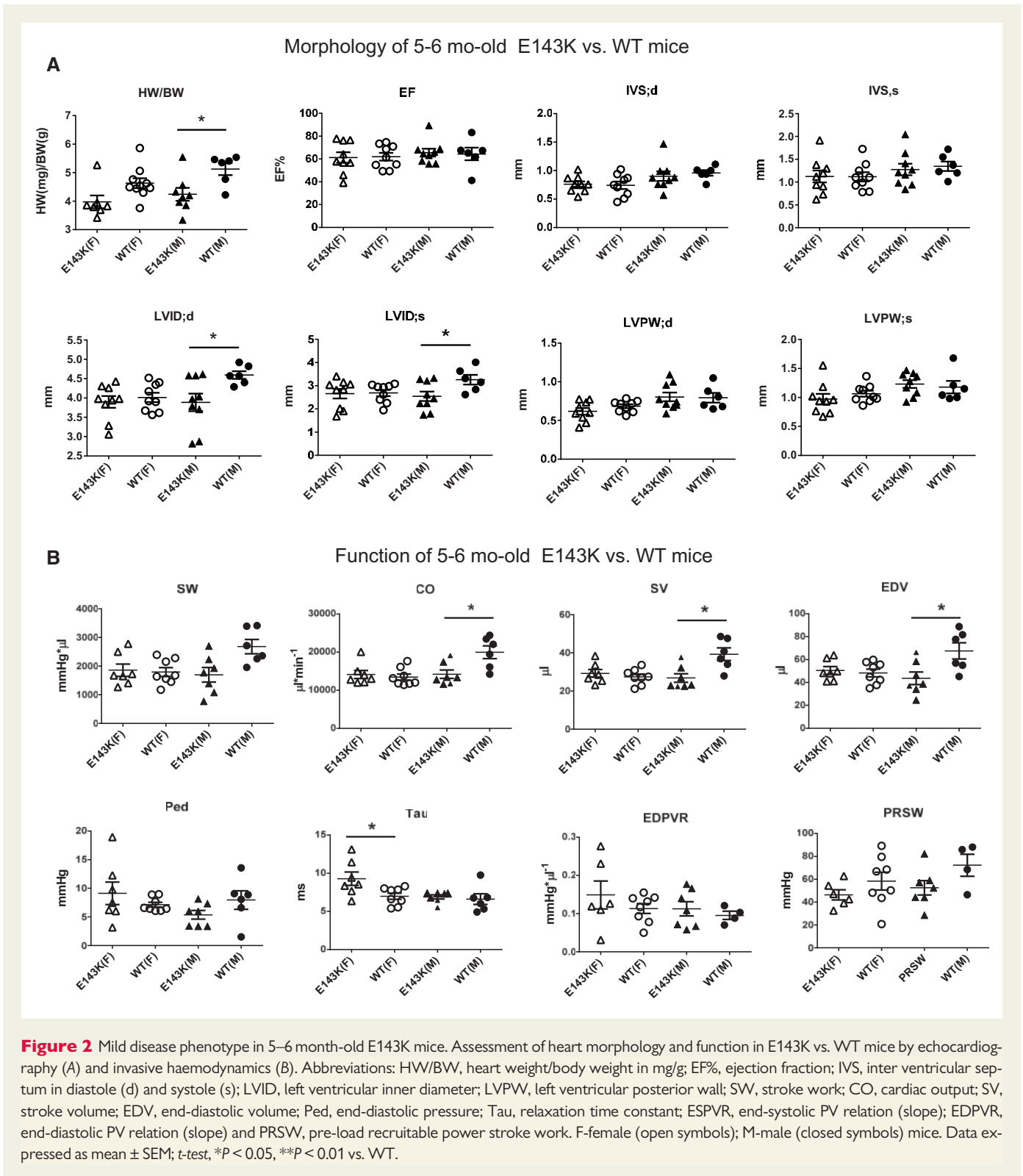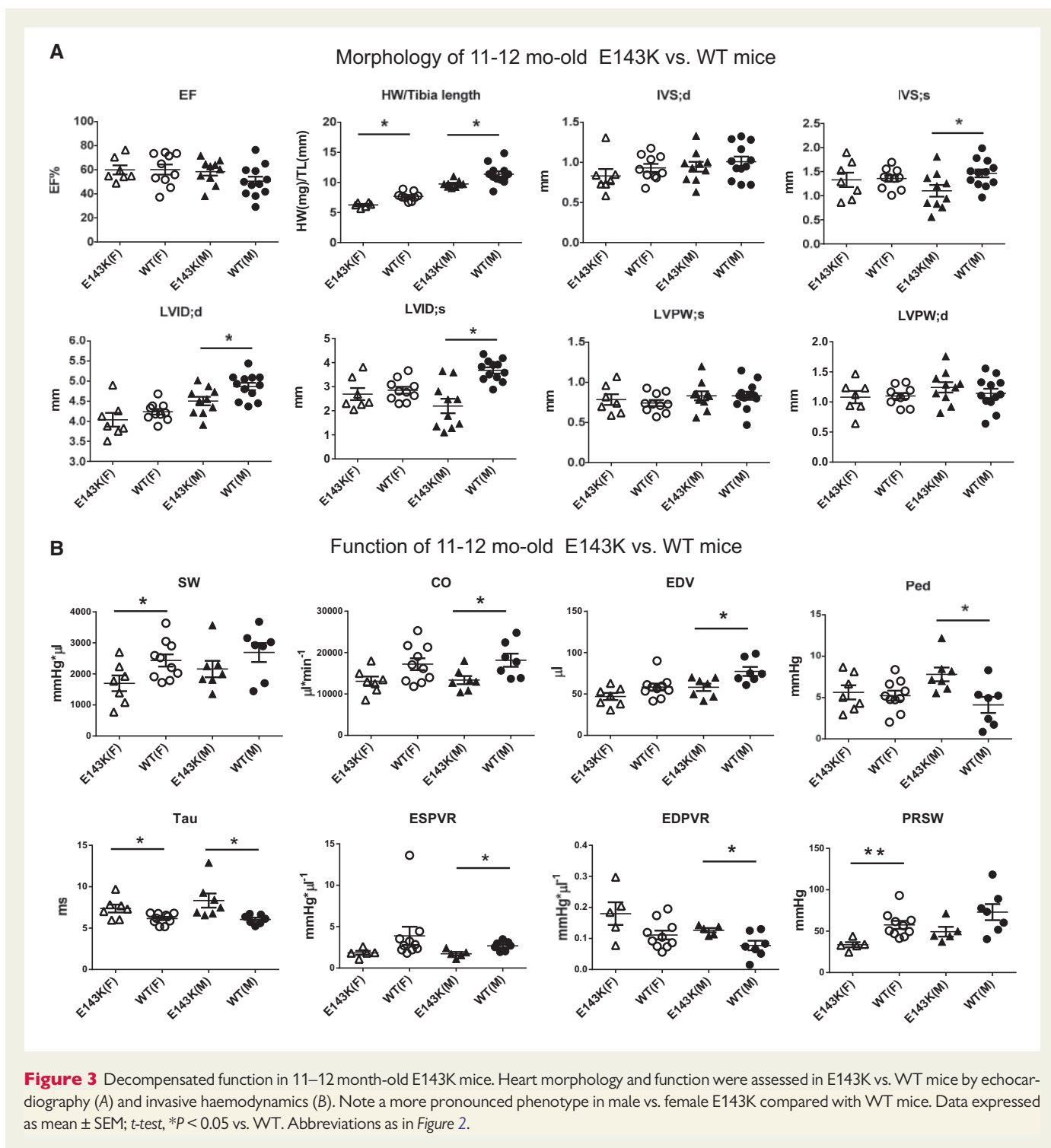
Figure 1 E143K mutation leads to time-dependent morphological changes in mice. (*A*) Histology and structure in representative E143K and WT hearts. H&E and Masson's trichrome stained LV sections from 5 to 6 (left) and 11 to 12 (right) mo-old female and male E143K mice compared with WT mice. Scale bar, 50 μm. (*B*) Electron microscopy images of 11 mo-old E143K vs. WT-hearts. Note Z-line streaming (arrowhead) and the areas with disorganized sarcomeric structures (asterisk) in E143K-hearts. Scale bars: 2 μm (upper panel), 1 μm (middle panel) and 0.2 μm (lower panel). (*C*) Hydroxyproline (HOP) content, and stress-related gene expression in E143K vs. WT hearts. HOP was measured in LV tissue from ∼11 mo-old E143K (2M, 3F) compared with WT (2M, 3F) mice. Expression of stress-related genes was assessed in ∼6 mo-old E143K (2M, 3F) compared with WT (2M, 3F) mice. M, blue symbols; F, red symbols. Data are presented as mean ±SEM, *t-test*, *$P < 0.05$ vs. WT.

Figure 2 Mild disease phenotype in 5–6 month-old E143K mice. Assessment of heart morphology and function in E143K vs. WT mice by echocardiography (*A*) and invasive haemodynamics (*B*). Abbreviations: HW/BW, heart weight/body weight in mg/g; EF%, ejection fraction; IVS, inter ventricular septum in diastole (d) and systole (s); LVID, left ventricular inner diameter; LVPW, left ventricular posterior wall; SW, stroke work; CO, cardiac output; SV, stroke volume; EDV, end-diastolic volume; Ped, end-diastolic pressure; Tau, relaxation time constant; ESPVR, end-systolic PV relation (slope); EDPVR, end-diastolic PV relation (slope) and PRSW, pre-load recruitable power stroke work. F-female (open symbols); M-male (closed symbols) mice. Data expressed as mean ± SEM; *t-test*, *P < 0.05, **P < 0.01 vs. WT.

myosin and a higher affinity of E143K-myosin to pyrene-actin (*Figure 5A*). Consistent with the hypercontractile mutant-myosin performance, the actin-activated myosin ATPase activity was higher for E143K compared with WT myosin (*Figure 5B*). The higher V_{max} indicated a faster transition from the weakly to strongly bound cross-bridges, with phosphate release being rate-limiting[22] in the mutant vs. WT myosin (*Figure 5B*), suggesting a mutation induced increase in the myosin duty ratio.[23] The

Michaelis–Menten constant for E143K myosin was not different from WT ($K_m = 1.14 \pm 0.10$ vs. $1.19 \pm 0.12 \mu M$). To further demonstrate the effect of E143K on interaction of myosin with actin, the MgATP-dependent transition from strongly (A·M) to weakly (A·M·ATP) bound acto-myosin complex was measured using pyrene-F-actin. E143K and WT myosins were stoichiometrically mixed with pyrene-F-actin and the complexes were mixed in a 1:1 (vol/vol) ratio with increasing

Figure 3 Decompensated function in 11–12 month-old E143K mice. Heart morphology and function were assessed in E143K vs. WT mice by echocardiography (*A*) and invasive haemodynamics (*B*). Note a more pronounced phenotype in male vs. female E143K compared with WT mice. Data expressed as mean ± SEM; *t-test*, *P < 0.05 vs. WT. Abbreviations as in *Figure 2*.

concentrations of MgATP (10–125 μM) in a stopped flow apparatus. An increase in pyrene fluorescence upon addition of MgATP was monitored as a function of time. The observed rate constant (k_{obs}) for the A·M → A·M·ATP transition plotted as a function of [MgATP] showed a significant decrease in the slope of k_{obs}-[MgATP] dependence for E143K vs. WT myosin, indicating a slower transition from strongly to weakly bound E143K-cross-bridges (*Figure 5C*). Individual acto-myosin dissociation rates, k_{obs}, for different ATP concentrations were also smaller in E143K myosin compared with WT (*Figure 5D*). A decrease in the rate of dissociation of acto-myosin complex by MgATP observed in E143K hearts could also be due to the downregulation of α-MHC (*Figure 1C*), thereby increased ratio of β-MHC/α-MHC in total MHC content of E143K hearts. Altogether, these data indicate that in the absence of nucleotide, E143K-ELC myosin elicits significantly stronger interactions with actin than WT myosin and decreases the rates of ATP dependent relaxation of the acto-myosin complex.
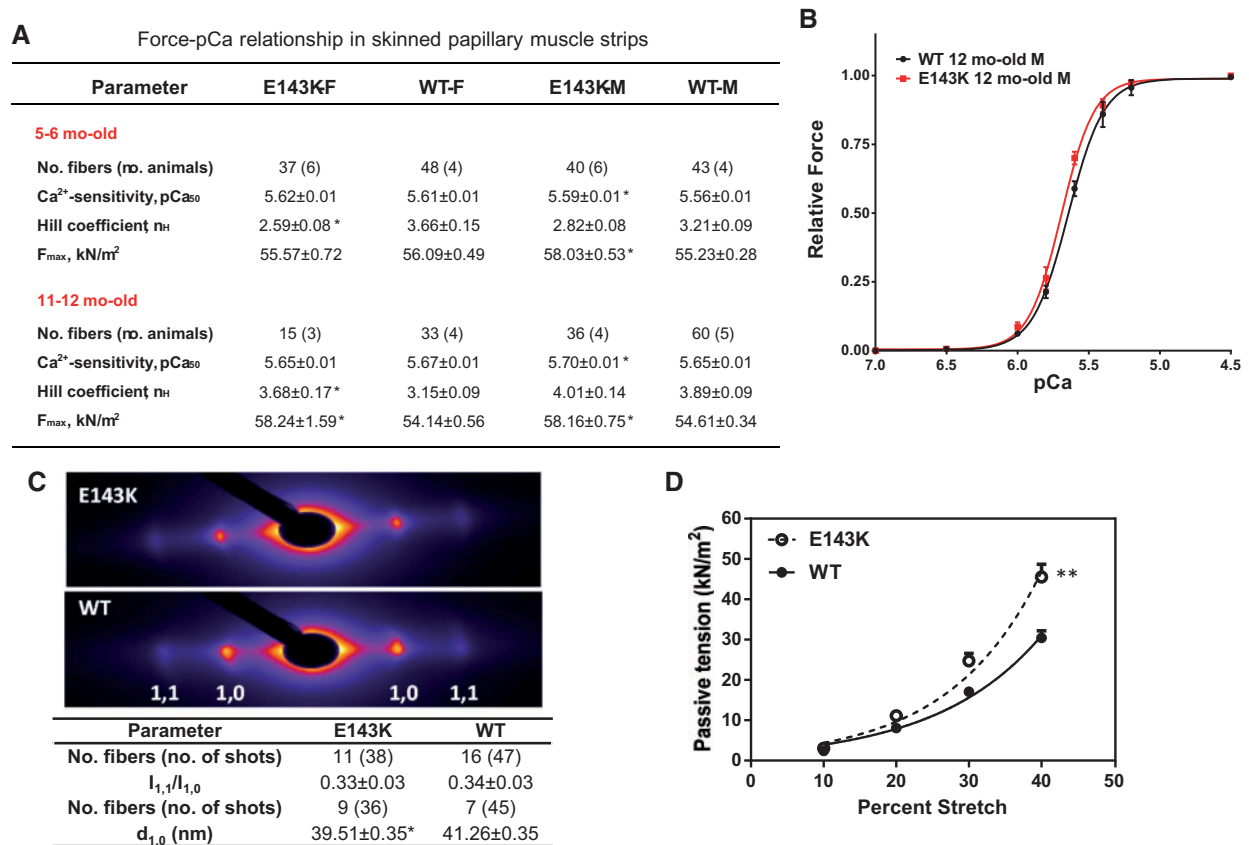
Figure 4 E143K-induced changes of function and sarcomere lattice in papillary muscle strips. (*A*) Development of steady-state force in skinned papillary muscle fibers from E143K vs. WT mice. Two age groups with 3–6 animals per group were used. (*B*) Representative force-pCa relationship in ~12 mo-old E143K-M vs. WT-M mice. (*C*) Fiber diffraction pattern in ~6 mo-old male E143K (4M, 2F) vs. WT (5M, 1F) mice under relaxation conditions (pCa 8). Lattice spacing $d_{1,0}$ (in nm) and equatorial reflections' intensity ratio $I_{1,1}/I_{1,0}$. Sarcomere length was 2.1 μm. Note a significant decrease in the lattice spacing in the mutant mice compared with WT mice. Data are expressed as average ± SEM of *n* (number of fibers) with *$P < 0.05$ vs. WT (*t-test*). (*D*) Passive tension measured in ~6 mo-old E143K (2M, 1F yielding 29 fibers) vs. WT (2F, 1M yielding 27 fibers). Note significantly higher passive tension measured in E143K vs. WT hearts as assessed by two-way ANOVA for repetitive measurements (**$P < 0.01$).

3.5 *In vitro* motility and Qdot study

V_{max} and K_m Michaelis–Menten parameters obtained at low ionic strength imitating *in vitro* motility conditions are summarized in Supplementary material online, *Table S3*. V_{max} increased two-fold for E143K over WT paralleling the trend at higher ionic strength (*Figure 5B*). *In vitro* motility velocity, v_m, saturated at ~0.1 μM myosin bulk concentration and converged to similar maximum velocities for WT and E143K-myosins. Maximum motility velocities are likewise summarized in Supplementary material online, *Table S3*. *Figures 6A, B* shows baseline subtracted event-velocity histograms of pooled data (solid squares connected with dashed line) for 21 and 27 acquisitions from WT and E143K and their simulation (solid lines). Peaks or inflection points appearing below 2 vu (velocity units) are short (↑red or S), intermediate (↓green or I), and long (↑ blue or L) step-sizes in nm. Steps in combination are also indicated. One-way ANOVA testing indicated that the short and long step-sizes were significantly different between WT and E143K-myosins. *Figures 6C* and *D* show the step-frequency (ω) expectations, expectation values, and standard deviations for the S, I, and L unitary steps estimated from simulation of data in *Figures A and B*. The expectation curves in *Figures C and D* indicate the relative probability

for step-frequency values along the abscissa. The area under the colour coded curves for the S, I, and L steps equals expectation values ω_S, ω_I, and ω_L, respectively. The sum $\omega_{S} + \omega_{I} + \omega_{L} = 1$ for each myosin species. One-way ANOVA testing indicated that WT and E143K step-frequencies are statistically identical in each category (short, intermediate, or long).

Average duty ratio, <*f*>, for the WT and E143K-myosins indicated in Supplementary material online, *Table S3* used the average step size <*d*> = $\omega_S\ d_S + \omega_I\ d_I + \omega_L\ d_L$, motility velocity v_m, and V_{max} in the expression <*f*> = V_{max} <*d*>/v_m. Results indicated a two-fold increase in duty ratio for E143K due to two-fold increase in V_{max} coupled with modest and compensating changes to <*d*> and v_m for the mutant compared with WT. These data are consistent with enhanced force production for heart tissues containing the mutant motor.

Data in *Figure 6* indicate that the mouse cardiac myosin moves actin with three unitary step-sizes. Actin binding of the ELC N-terminus plays a central role in the mechanism for generating the short and long myosin step-sizes.[16,24] As shown, E143K mutation reduces step-size in the short and long steps implicating the ELC N-terminus actin binding interaction.
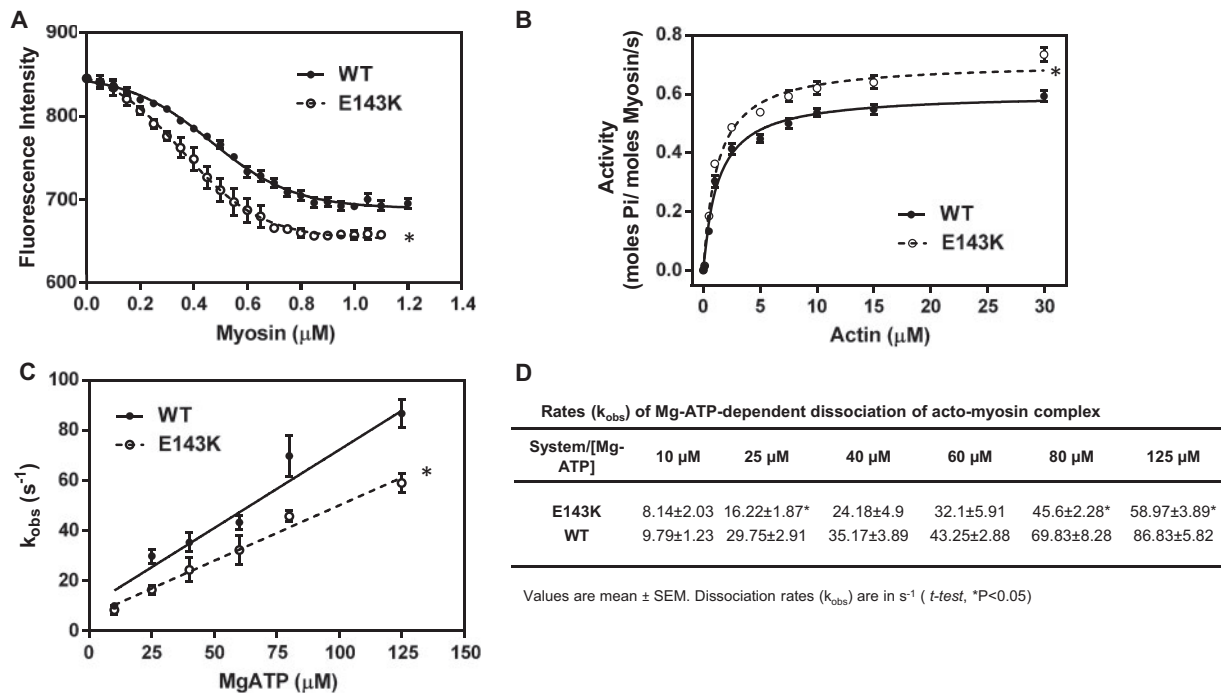
Figure 5 Hypercontractile activity of E143K myosin. (*A*) Fluorescence-based binding assays of E143K or WT myosin to pyrene-labeled F-actin. Note two different profiles of binding and a higher affinity of E143K myosin ($K_d = 0.368 \pm 0.09\ \mu M$, $n = 4$ curves performed in triplicate) for pyrene-actin compared with WT ($K_d = 0.465 \pm 0.138\ \mu M$, $n = 4$). (*B*) Actin-activated myosin ATPase activity of E143K and WT myosins. A significantly higher V_{max} was observed for E143K ($0.721 \pm 0.015\ s^{-1}$, $n = 13$) vs. WT ($0.615 \pm 0.014\ s^{-1}$, $n = 11$) myosin. The assays were performed in triplicate. (*C*) Stopped-flow assessment of k_{obs}-[MgATP] dependence and the rates of dissociation of the acto-myosin complex in E143K vs. WT mice. The effective second order MgATP binding rates measured by the slope of 'k_{obs}-[MgATP]' were: $0.444 \pm 0.039 \times 10^6\ M^{-1}\ s^{-1}$, $n = 4$ for E143K, and $0.626 \pm 0.068 \times 10^6\ M^{-1}\ s^{-1}$, $n = 3$ for WT, and the difference was statistically significant (*t-test*, $P = 0.0259$). (*D*) Dissociation rates (k_{obs}) for individual MgATP concentrations for E143K vs. WT myosin dissociating from pyrene-labeled F-actin. Measurements were performed on myosin extracted from the left and right ventricles of 4–8 mo-old female and male E143K and WT mice. Approx. 5 hearts/per group were used to generate one batch of myosin and the experiments were repeated with 2–4 different batches of myosin. Data are presented as mean ± SEM, *t-test*, *$P < 0.05$ vs. WT.

3.6 Metabolic and structural changes and protein phosphorylation in E143K vs. WT hearts

To understand the signalling triggers of RCM in E143K mice and capture relatively early changes in the metabolic/structural makeup of E143K vs. WT hearts, 3.6 mo-old F mice from both groups were subjected to an in-depth proteomic analysis. The reason that female mice have been chosen were recent studies showing that in all cardiomyopathy subtypes, there was an unequal sex distribution, with a tendency towards men for HCM and DCM, and towards women for RCM.[25] Reports also showed that under disease conditions, females have higher expression of genes related to energy metabolism and can better maintain their metabolic function in response to a disease stimulus than males.[26]

The data revealed that out of 758 identified proteins, 43 were differently expressed between E143K and WT mice (*Figure 7A*, see Supplementary material online, *Table S4*). The majority of upregulated proteins in E143K hearts was involved in ATP production and in mitochondrial metabolism. Consistent with a fatty acid to glucose metabolism pathway shift under stress or pathological conditions,[27,28] hexokinase-1,2 (G3UVV4, HXK2) proteins, responsible for glucose metabolism and the glycolytic ATP production pathway, were upregulated in E143K. Upstream of the β-oxidation of fatty acid (FA), acyl coenzyme A synthetase1 (ACSL1) and carnitine O-palmitoyltransferase 1 (CPT1b), that are responsible for activation and translocation of FA into mitochondria,[29–31] were upregulated in E143K-animals. In addition, carnitine O-acetyltransferase (CACP), responsible for transporting acetyl-carnitine out of the mitochondria and inhibiting FA oxidation,[32] was also upregulated in E143K-mice (*Figure 7B*). Several mitochondrial membrane proteins, including complex I (NADH dehydrogenase) subunits (NADUS2, NADUA9, NSUAA and NDUS1),[33] which are responsible for the electron transport and proton gradient across the membrane for ATP production,[34] were upregulated in E143K-mice. Fatty acid transport metabolites (CPT1b, CACP) and the voltage dependent anion channel (VDAC1), involved in the transport of anions, cations and metabolites across the outer membrane of mitochondria,[35,36] were all upregulated in the mutant mice. Upregulation of VDAC1 was confirmed by western blot performed on LV samples from E143K vs. WT (*Figure 7C, D*). Based upon the resolution of quantitative proteomics that was used in this study, the E143K elicited changes, although small, are likely to be biologically important and may underlie the molecular signatures of RCM-ELC hearts.

Interestingly, sarcomeric proteins such as cardiac TnI, TnT, ventricular myosin regulatory light chain (RLC) and α-MHC were downregulated while desmin was upregulated in the RCM model compared with WT
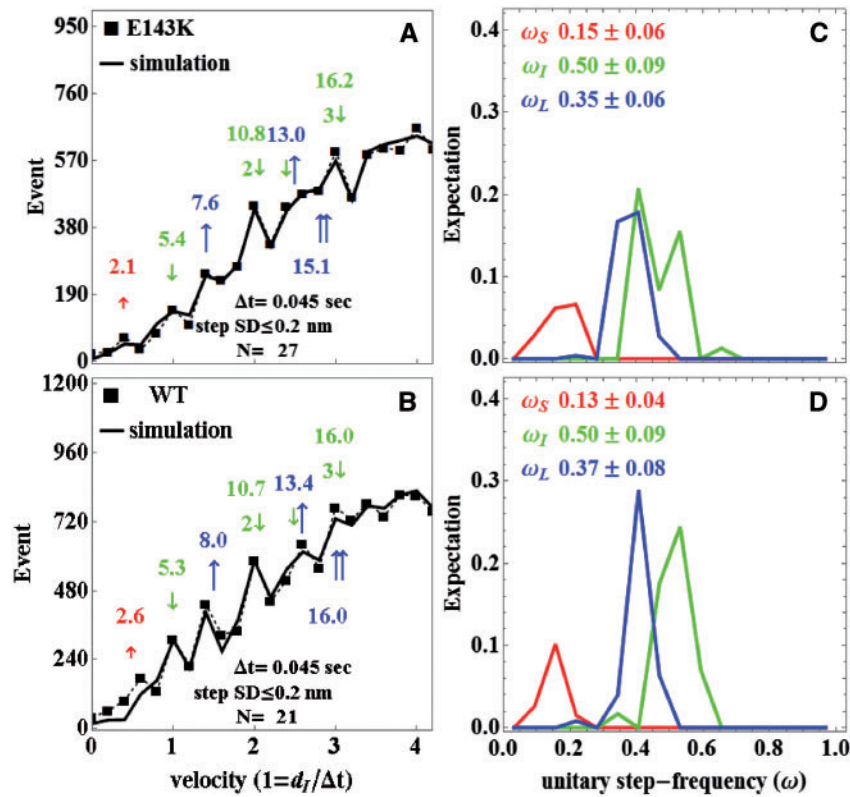
Figure 6 Stepping patterns of myosin motors in E143K and WT mice. Qdot motility assay was used to measure step-size and step-frequency for E143K and WT myosin. Panels (A) and (B) show baseline subtracted event-velocity histograms (solid squares connected by dashed line) for E143K and WT myosins with short (↑ red), intermediate (↓ green), and long (↑ blue) unitary step-sizes and their combination. Natural velocity units (vu) have $1 = d_I/\Delta t$ for the intermediate step-size divided by frame capture interval. Unitary steps and their combination are colour coded and indicated in nm above or below the event-velocity histogram. Simulations of the event-velocity histograms, providing the best estimates for step-size and step-frequencies as described in the text, are indicated with solid lines. Panels (C) and (D) indicate step-frequency expectations for E143K (C) and WT (D) myosins. Expectation values ω_S, ω_I, and ω_L are the areas under the curves for the short, intermediate, and long steps, respectively. Errors are standard deviation for 21 and 27 acquisitions from two batches of WT or E143K myosin.

(see Supplementary material online, *Table S4*). Downregulation of α-MHC was confirmed by real-time qPCR (*Figure 1C*). We also tested the effect of E143K on phosphorylation of cardiac TnI and myosin RLC (see Supplementary material online, *Figure S3*). The data were acquired using cardiac myofibrils isolated from three-age groups (2–3, 5–6, and 10–11 mo-old, females and males) of E143K vs. WT mice. A significantly lower RLC phosphorylation was observed in 2–3 mo-old and 5–6 mo-old E143K compared with WT animals (see Supplementary material online, *Figure S3*). Decreased phosphorylation in 10–11 mo-old E143K vs. WT mice did not reach statistical significance. At the same time, no changes in TnI phosphorylation was observed. One has to note that small increases in maximal tension and calcium sensitivity of force observed in E143K papillary fibers (*Figure 4*) would likely have been larger in the absence of counteracting activity of the poorly phosphorylated RLC.

Collectively, our results demonstrate that a charge modification (glutamic acid → lysine) on the ELC significantly changes the intermolecular interactions between ELC and the myosin heavy chain and between the myosin cross-bridges and actin and triggers an abnormal ability of myosin to generate the power stroke and muscle contraction. This hypercontractile activity of myosin ultimately leads to abnormalities in cardiac

systolic and diastolic function and morphology, and induces metabolic reprogramming in the E143K hearts.

4. Discussion

Genetic mutations in cardiac myosin light chains (ELC and RLC) are known to cause familial HCM with asymmetric septal hypertrophy and frequent occurrences of sudden cardiac death.[37] Several HCM-linked ELC mutations were studied in Tg mice,[11,38] but this study is the first to address the molecular mechanism of E143K-induced RCM in mice and the degree to which the phenotype resembles that observed in E143K-positive patients.[9,10] Our data indicate that despite ∼55% incorporation of E143K into the hearts of mice, we were able to recapitulate the major aspects of human RCM (e.g. diastolic disturbance, interstitial fibrosis), whose pronounced phenotype could only be observed in homozygous E143K-patients.[10] Male and female mutant mice manifested mildly altered morphology and function at 5–6 months of age and significantly progressed to severely defective morphology at 11–12 months. Throughout the life, the hearts of mutant-animals have not hypertrophied and with the
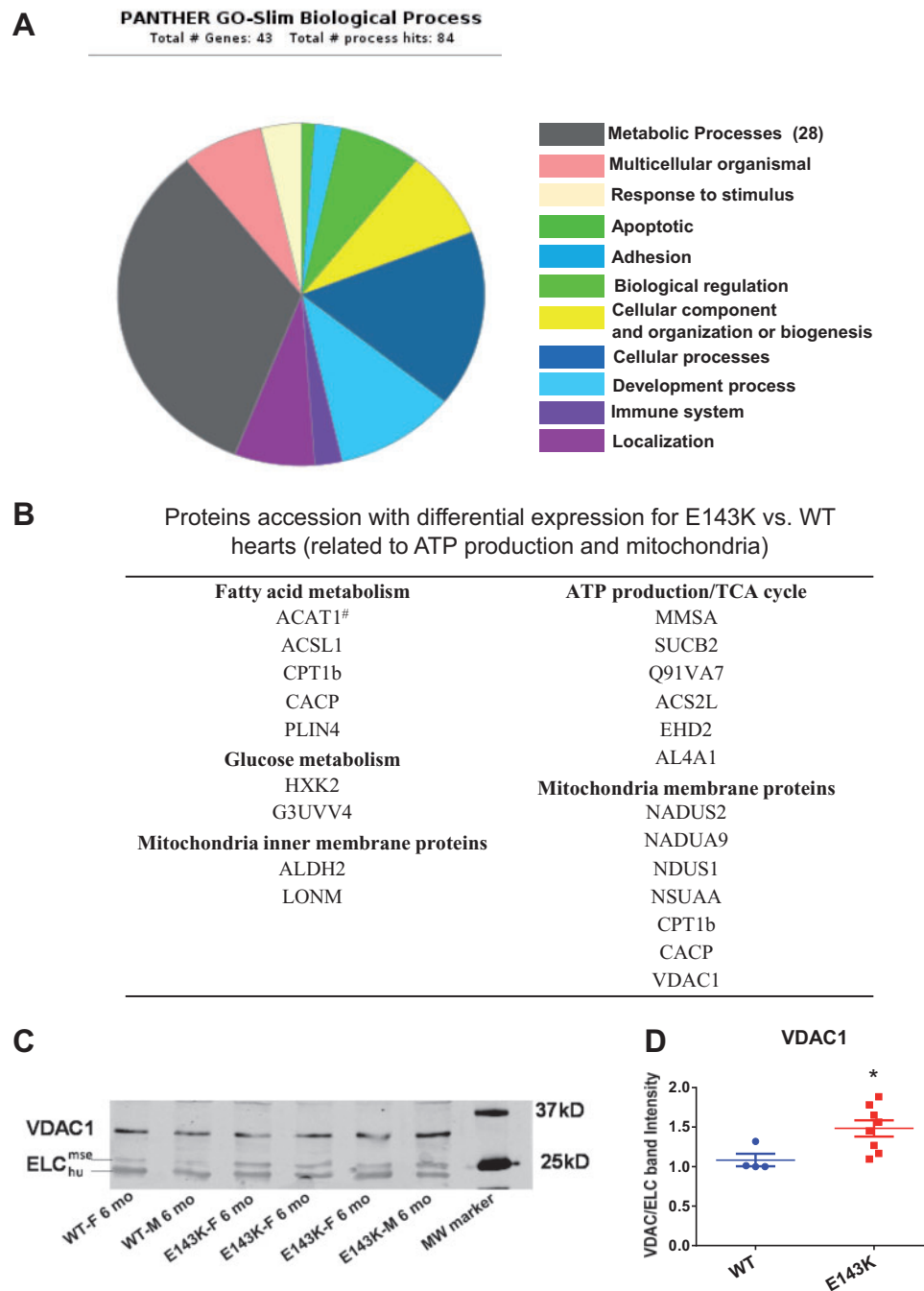
Figure 7 Protein expression changes in E143K vs. WT hearts. (*A*) Biological processes affected in E143K animals. A total of 43 proteins had differential expression in E143K-hearts compared with WT. The major differentially expressed proteins are those involved in metabolic processes. (*B*) Proteins related to mitochondrial content and ATP production that were differentially expressed in E143K vs. WT mice. # indicates a downregulated protein vs. all other upregulated proteins. (*C*) Western blot and (*D*) Quantification of VDAC1 expression confirming proteomic data. Data are mean ± SEM, *t-test*, *$P < 0.05$ vs. WT.

exception of older E143K-F, the hearts of F and M E143K-mice became significantly smaller compared with age and gender matched WT mice. It is important to note that male (young and old) E143K-mice showed more evidence of disease than their female counterparts, a phenomenon also observed in other models of genetic cardiomyopathy.[19,26]

In humans, gender differences are clearly observed at every level of cardiovascular physiology from action potential duration, mitochondrial energetics to isolated muscle fibre and whole-heart contractile function.[19] As observed in our study with 5–6 mo-old female E143K mice showing mild detrimental cardiac changes compared with age matched male counterparts and to senescent F and M mice, studies in humans

revealed that cardioprotection, that is present in younger women, is generally lost later in life, suggesting a role for estrogen in cardiovascular biology. In animal studies, estrogen was shown to protect from Ang II-induced hypertrophy in ovariectomized mice supplemented with estrogen during Ang II treatment.[39] This protection in female mice, however, was lost with depletion of endogenous sex hormones. Consistent with our results, significant sex differences were also found in a mouse model of TAC showing a more pronounced increase in myocardial hypertrophy and fibrosis in male animals.[26] Interestingly, treatment with E2, a major circulating estrogen, has been shown to inhibit LV hypertrophy and prohypertrophic gene expression in the TAC model.[40] These reports suggest that females E143K mice may be protected against effects of RCM and thus demonstrate a milder phenotype of disease that males (*Figures 2–4*).

Cardiac fibrosis is a hallmark of HCM that largely contributes to arrhythmias and heart failure and evidence is accumulating for increased ratios of collagen synthesis to degradation in HCM patients.[41] Studies on humans and animal models indicate that profibrotic gene pathways can be activated much earlier than hypertrophic cardiac remodelling, and increased myocardial collagen synthesis was observed in sarcomere mutation carriers prior to the development of LV hypertrophy and fibrosis.[41] Consistent with these reports, 5–6 mo-old E143K-mice showed mild fibrosis while collagen type I and III genes were upregulated (*Figure 1A, C*). Therefore, in addition to symptom-based treatments of RCM patients with diuretics to decrease filling pressures, beta-blockers and angiotensin-converting enzyme (ACE) inhibitors, the synthesis of collagen has been targeted.[5] In fact, many of the beta-blockers and ACE inhibitors (e.g. valsartan) were shown to suppress the synthesis of type I collagen in patients with HCM.[42] Altogether, these treatments of RCM and anti-fibrosis in particular hold promise in that cardiac transplantation, despite currently being the most effective procedure in treating RCM,[5] is not a sole solution to the problem.

Studies in E143K papillary muscle fibers, that are pre-dominantly free of fibrotic depositions,[21] showed an increased ability of myosin to generate maximal force supporting the idea of E143K-induced pathological hypercontractile state of myosin motor (*Figure 4A*). Likewise, E143K myosin showed a higher affinity for actin under rigor conditions which, when placed *in vivo*, could contribute to increased LV stiffness and cause abnormal resistance to ventricular filling and diastolic disturbance. The hypercontractility-like state observed in E143K mice was also evident in acto-myosin interaction with significantly higher actin-activated ATPase activity and increased myosin duty ratio measured in E143K vs. WT preparations. Consistent with these data, the rates of ATP-dependent dissociation of the acto-myosin complex were slower in E143K compared with WT mice, indicating a slower transition from the strongly to weakly bound myosin cross-bridges (*Figure 5*). Accordingly, single molecule studies demonstrated a large increase in the duty ratio for E143K vs. WT myosin, supporting the hypercontractile E143K-phenotype (see Supplementary material online, *Table S3*). Augmented maximal tension could also be due to increased muscle stiffness that would result in impaired muscle relaxation and ultimately in diastolic dysfunction. In line with this, X-ray measurements revealed a significant decrease in the lattice spacing in E143K vs. WT fibers under relaxation conditions (pCa 8) (*Figure 4C*). Reduced $d_{1,0}$ may indicate that the E143K-thick filaments become closer to the thin filaments facilitating the interaction of myosin with actin and promoting generation of force. Likewise, passive tension measured under relaxation conditions was increased in the mutant vs. WT mice, and this change is expected to contribute to increased stiffness in E143K myocardium (*Figure 4D*).

Our data on phosphorylation of cardiac TnI and myosin RLC, acquired in myofibrils from 2 to 3, 5 to 6, and 10 to 11 mo-old E143K vs. WT mice, revealed a significantly reduced phosphorylation of RLC with no changes in TnI phosphorylation in the mutant (see Supplementary material online, *Figure S3*). Thus, it is possible that small increases in maximal tension and calcium sensitivity of force observed in E143K papillary fibers would have been larger in the absence of counteracting activity of the poorly phosphorylated RLC. There is a large body of evidence showing that reduced RLC phosphorylation may result in abnormal heart performance in mice[43,44] and in men,[45] presumably through morphological and/or myofibrillar functional alterations (e.g. change in force, myofilament calcium sensitivity, ATPase activity, cross-bridge kinetics). Likewise, attenuation of RLC phosphorylation in cMLCK knock-out mice was demonstrated to cause ventricular hypertrophy, fibrosis, and DCM.[46] Consistent with these data, no increase in $I_{1,1}/I_{1,0}$ ratio was observed in E143K fibers, the result which is in accord with minute changes in Ca^{2+}-sensitivity of force (*Figure 4A–C*). Therefore, reduced RLC phosphorylation most likely contributes to E143K-RCM phenotype and may represent a novel target for drug therapy.[14,23]

Proteomic studies demonstrated a mutation-induced abnormal metabolic makeup in E143K vs. WT hearts with changes in the processes involving ATP production and expression of energy related mitochondrial proteins. Disruption of the metabolic function of the heart is known to lead to cardiac (diastolic and systolic) abnormalities and development of cardiomyopathy,[47] and our data are in line with those showing the transition from a fatty acid metabolism to glucose metabolism pathway in the heart subjected to the pathologic stress.[27,28] This pathological reprogramming of the E143K hearts was also evident by the upregulation of certain mitochondrial proteins including the ATP producing enzymes. Upregulation of several subunits of complex I, which plays a key role in cellular energy production by transferring electrons from NADH to ubiquinone,[33] were monitored in E143K vs. WT hearts. Most likely, the E143K mutated hearts with their abnormally stiff ventricles exhibit a high demand for ATP to sustain the hypercontractile myosin cross-bridge cycling (increased ATPase activity) leading to the pathological generation of force. Ultimately, metabolically compromised E143K hearts were unable to compensate for the abnormal energy demand resulting in more complex cardiac defects and systolic dysfunction as observed in older mutant hearts.

Mechanistically, as a result of E143K-induced charge change on myosin ELC, the interaction of ELC with the myosin heavy chain and possibly with myosin RLC was significantly altered leading to changes in the steady-state and kinetics of acto-myosin interactions. These changes combined with alterations in sarcomeric protein phosphorylation and cellular accumulation of collagen resulted in structural and functional defects in E143K mice evidenced by stiffened ventricles and physiological, morphologic and metabolic remodelling consistent with the development of RCM in humans. This hypercontractility of myosin motor and its abnormal ability to generate the power stroke and muscle contraction is hypothesized to underlie the development of cardiac defects in E143K mice. Consistent with our data, modulation of force generation and stiffness of myosin motors by ELC and HCM-ELC mutations was recently shown by the Morano group.[38] Altogether, the experimental data suggest that our RCM-ELC mouse model may be highly suitable for testing of novel myosin specific therapeutics[23] aimed to normalize the myosin motor function, decrease pathological power production, and avert the hypercontractile state of the heart.

Supplementary material

Supplementary material is available at *Cardiovascular Research* online.

Conflict of interest: none declared.

Funding

References

1. Maron BJ, Towbin JA, Thiene G, Antzelevitch C, Corrado D, Arnett D, Moss AJ, Seidman CE, Young JB, American Heart A, Council on Clinical Cardiology HF, Transplantation C, Quality of C, Outcomes R, Functional G, Translational Biology Interdisciplinary Working G, Council on E, Prevention. Contemporary definitions and classification of the cardiomyopathies: an American Heart Association Scientific Statement from the Council on Clinical Cardiology, Heart Failure and Transplantation Committee; Quality of Care and Outcomes Research and Functional Genomics and Translational Biology Interdisciplinary Working Groups; and Council on Epidemiology and Prevention. *Circulation* 2006;**113**:1807–1816.

2. Kaski JP, Syrris P, Burch M, Tomé-Esteban M-T, Fenton M, Christiansen M, Andersen PS, Sebire N, Ashworth M, Deanfield JE, McKenna WJ, Elliott PM. Idiopathic restrictive cardiomyopathy in children is caused by mutations in cardiac sarcomere protein genes. *Heart* 2008;**94**:1478–1484.

3. Kushwaha SS, Fallon JT, Fuster V. Restrictive cardiomyopathy. *N Engl J Med* 1997;**336**:267–276.

4. van der Velden J, Ho CY, Tardiff JC, Olivotto I, Knollmann BC, Carrier L. Research priorities in sarcomeric cardiomyopathies. *Cardiovasc Res* 2015;**105**:449–456.

5. Jean-Charles PY, Li YJ, Nan CL, Huang XP. Insights into restrictive cardiomyopathy from clinical and animal studies. *J Geriatr Cardiol* 2011;**8**:168–183.

6. Rivenes SM, Kearney DL, Smith EOB, Towbin JA, Denfield SW. Sudden death and cardiovascular collapse in children with restrictive cardiomyopathy. *Circulation* 2000;**102**:876–882.

7. Li Y, Zhang L, Jean-Charles PY, Nan C, Chen G, Tian J, Jin JP, Gelb IJ, Huang X. Dose-dependent diastolic dysfunction and early death in a mouse model with cardiac troponin mutations. *J Mol Cell Cardiol* 2013;**62**:227–236.

8. Karam S, Raboisson MJ, Ducreux C, Chalabreysse L, Millat G, Bozio A, Bouvagnet P. A de novo mutation of the beta cardiac myosin heavy chain gene in an infantile restrictive cardiomyopathy. *Congenit Heart Dis* 2008;**3**:138–143.

9. Caleshu C, Sakhuja R, Nussbaum RL, Schiller NB, Ursell PC, Eng C, De Marco T, McGlothlin D, Burchard EG, Rame JE. Furthering the link between the sarcomere and primary cardiomyopathies: restrictive cardiomyopathy associated with multiple mutations in genes previously associated with hypertrophic or dilated cardiomyopathy. *Am J Med Genet A* 2011;**155**:2229–2235.

10. Olson TM, Karst ML, Whitby FG, Driscoll DJ. Myosin light chain mutation causes autosomal recessive cardiomyopathy with mid-cavitary hypertrophy and restrictive physiology. *Circulation* 2002;**105**:2337–2340.

11. Kazmierczak K, Paulino EC, Huang W, Muthu P, Liang J, Yuan CC, Rojas AI, Hare JM, Szczesna-Cordary D. Discrete effects of A57G-myosin essential light chain mutation associated with familial hypertrophic cardiomyopathy. *Am J Physiol Heart Circ Physiol* 2013;**305**:H575–589.

12. Kazmierczak K, Xu Y, Jones M, Guzman G, Hernandez OM, Kerrick WGL, Szczesna-Cordary D. The role of the N-terminus of the myosin essential light chain in cardiac muscle contraction. *J Mol Biol* 2009;**387**:706–725.

13. Muthu P, Wang L, Yuan CC, Kazmierczak K, Huang W, Hernandez OM, Kawai M, Irving TC, Szczesna-Cordary D. Structural and functional aspects of the myosin essential light chain in cardiac muscle contraction. *FASEB J* 2011;**25**:4394–4405.

14. Yuan CC, Muthu P, Kazmierczak K, Liang J, Huang W, Irving TC, Kanashiro-Takeuchi RM, Hare JM, Szczesna-Cordary D. Constitutive phosphorylation of cardiac myosin regulatory light chain prevents development of hypertrophic cardiomyopathy in mice. *Proc Natl Acad Sci U S A* 2015;**112**:E4138–4146.

15. Wang Y, Ajtai K, Burghardt TP. Analytical comparison of natural and pharmaceutical ventricular myosin activators. *Biochemistry* 2014;**53**:5298–5306.

16. Wang Y, Ajtai K, Kazmierczak K, Szczesna-Cordary D, Burghardt TP. N-terminus of cardiac myosin essential light chain modulates myosin step-size. *Biochemistry* 2015;**55**:186–198.

17. Burghardt TP, Sun X, Wang Y, Ajtai K. In vitro and in vivo single myosin step-sizes in striated muscle. *J Muscle Res Cell Motil* 2015;**36**:463–477.

18. Gomes AV, Kazmierczak K, Cheah JX, Gilda JE, Yuan CC, Zhou Z, Szczesna-Cordary D. Proteomic analysis of physiological versus pathological cardiac remodeling in animal models expressing mutations in myosin essential light chains. *J Muscle Res Cell Motil* 2015;**36**:447–461.

19. Blenck CL, Harvey PA, Reckelhoff JF, Leinwand LA. The importance of biological sex and estrogen in rodent models of cardiovascular health and disease. *Circ Res* 2016;**118**:1294–1312.

20. Wang L, Muthu P, Szczesna-Cordary D, Kawai M. Characterizations of myosin essential light chain's N-terminal truncation mutant Delta43 in transgenic mouse papillary muscles by using tension transients in response to sinusoidal length alterations. *J Muscle Res Cell Motil* 2013;**34**:93–105.

21. Wang Y, Xu Y, Kerrick WGL, Wang Y, Guzman G, Diaz-Perez Z, Szczesna-Cordary D. Prolonged Ca^{2+} and force transients in myosin RLC transgenic mouse fibers expressing malignant and benign FHC mutations. *J Mol Biol* 2006;**361**:286–299.

22. He ZH, Chillingworth RK, Brune M, Corrie JE, Trentham DR, Webb MR, Ferenczi MA. ATPase kinetics on activation of rabbit and frog permeabilized isometric muscle fibres: a real time phosphate assay. *J Physiol* 1997;**501**:125–148.

23. Green EM, Wakimoto H, Anderson RL, Evanchik MJ, Gorham JM, Harrison BC, Henze M, Kawas R, Oslob JD, Rodriguez HM, Song Y, Wan W, Leinwand LA, Spudich JA, McDowell RS, Seidman JG, Seidman CE. A small-molecule inhibitor of sarcomere contractility suppresses hypertrophic cardiomyopathy in mice. *Science* 2016;**351**:617–621.

24. Wang Y, Ajtai K, Burghardt TP. Qdot labeled actin super-resolution motility assay measures low duty cycle muscle myosin step-size. *Biochemistry* 2013;**52**:1611–1621.

25. Elliott P, Charron P, Blanes JR, Tavazzi L, Tendera M, Konte M, Laroche C, Maggioni AP, Investigators ECRP. European cardiomyopathy pilot registry: EURObservational research programme of the European society of cardiology. *Eur Heart J* 2016;**37**:164–173.

26. Regitz-Zagrosek V, Kararigas G. Mechanistic pathways of sex differences in cardiovascular disease. *Physiol Rev* 2017;**97**:1–37.

27. Kolwicz SC, Purohit S, Tian R. Cardiac metabolism and its interactions with contraction, growth, and survival of cardiomyocytes. *Circ Res* 2013;**113**:603–616.

28. Lionetti V, Stanley WC, Recchia FA. Modulating fatty acid oxidation in heart failure. *Cardiovasc Res* 2011;**90**:202–209.

29. Black PN, DiRusso CC. Transmembrane movement of exogenous long-chain fatty acids: proteins, enzymes, and vectorial esterification. *Microbiol Mol Biol Rev* 2003;**67**:454–472.

30. Ellis JM, Mentock SM, DePetrillo MA, Koves TR, Sen S, Watkins SM, Muoio DM, Cline GW, Taegtmeyer H, Shulman GI, Willis MS, Coleman RA. Mouse cardiac acyl coenzyme a synthetase 1 deficiency impairs fatty acid oxidation and induces cardiac hypertrophy. *Mol Cell Biol* 2011;**31**:1252–1262.

31. Yamazaki N, Shinohara Y, Shima A, Terada H. High expression of a novel carnitine palmitoyltransferase I like protein in rat brown adipose tissue and heart: isolation and characterization of its cDNA clone. *FEBS Lett* 1995;**363**:41–45.

32. Abo Alrob O, Lopaschuk Gary D. Role of CoA and acetyl-CoA in regulating cardiac fatty acid and glucose oxidation. *Biochem Soc Trans* 2014;**42**:1043–1051.

33. Fiedorczuk K, Letts JA, Degliesposti G, Kaszuba K, Skehel M, Sazanov LA. Atomic structure of the entire mammalian mitochondrial complex I. *Nature* 2016;**538**:406–410.

34. Weiss H, Friedrich T, Hofhaus G, Preis D. The respiratory-chain NADH dehydrogenase (complex I) of mitochondria. *Eur J Biochem* 1991;**197**:563–576.

35. Tan W, Colombini M. VDAC closure increases calcium ion flux. *Biochim Biophys Acta* 2007;**1768**:2510–2515.

36. Rostovtseva TK, Bezrukov SM. VDAC regulation: role of cytosolic proteins and mitochondrial lipids. *J Bioenerg Biomembr* 2008;**40**:163–170.

37. Poetter K, Jiang H, Hassanzadeh S, Master SR, Chang A, Dalakas MC, Rayment I, Sellers JR, Fananapazir L, Epstein ND. Mutations in either the essential or regulatory light chains of myosin are associated with a rare myopathy in human heart and skeletal muscle. *Nat Genet* 1996;**13**:63–69.

38. Lossie J, Kohncke C, Mahmoodzadeh S, Steffen W, Canepari M, Maffei M, Taube M, Larcheveque O, Baumert P, Haase H, Bottinelli R, Regitz-Zagrosek V, Morano I. Molecular mechanism regulating myosin and cardiac functions by ELC. *Biochem Biophys Res Commun* 2014;**450**:464–469.

39. Pedram A, Razandi M, Lubahn D, Liu J, Vannan M, Levin ER. Estrogen inhibits cardiac hypertrophy: role of estrogen receptor-beta to inhibit calcineurin. *Endocrinology* 2008;**149**:3361–3369.

40. van Eickels M, Grohe C, Cleutjens JP, Janssen BJ, Wellens HJ, Doevendans PA. 17beta-estradiol attenuates the development of pressure-overload hypertrophy. *Circulation* 2001;**104**:1419–1423.

41. Ho CY, Lopez B, Coelho-Filho OR, Lakdawala NK, Cirino AL, Jarolim P, Kwong R, Gonzalez A, Colan SD, Seidman JG, Diez J, Seidman CE. Myocardial fibrosis as an

early manifestation of hypertrophic cardiomyopathy. *N Engl J Med* 2010;**363**:552–563.

42. Kawano H, Toda G, Nakamizo R, Koide Y, Seto S, Yano K. Valsartan decreases type I collagen synthesis in patients with hypertrophic cardiomyopathy. *Circ J* 2005;**69**:1244–1248.

43. Huang W, Liang J, Kazmierczak K, Muthu P, Duggal D, Farman GP, Sorensen L, Pozios I, Abraham T, Moore JR, Borejdo J, Szczesna-Cordary D. Hypertrophic cardiomyopathy associated Lys104Glu mutation in the myosin regulatory light chain causes diastolic disturbance in mice. *J Mol Cell Cardiol* 2014;**74**:318–329.

44. Kerrick WGL, Kazmierczak K, Xu Y, Wang Y, Szczesna-Cordary D. Malignant familial hypertrophic cardiomyopathy D166V mutation in the ventricular myosin regulatory light chain causes profound effects in skinned and intact papillary muscle fibers from transgenic mice. *FASEB J* 2009;**23**:855–865.

45. van der Velden J, Papp Z, Boontje NM, Zaremba R, de Jong JW, Janssen PML, Hasenfuss G, Stienen GJM. The effect of myosin light chain 2 dephosphorylation on Ca^{2+}-sensitivity of force is enhanced in failing human hearts. *Cardiovasc Res* 2003;**57**:505–514.

46. Ding P, Huang J, Battiprolu PK, Hill JA, Kamm KE, Stull JT. Cardiac myosin light chain kinase is necessary for myosin regulatory light chain phosphorylation and cardiac performance in vivo. *J Biol Chem* 2010;**285**:40819–40829.

47. Doenst T, Nguyen TD, Abel ED. Cardiac metabolism in heart failure: implications beyond ATP production. *Circ Res* 2013;**113**:709–724.